Investigation of Stresses in Coal Gasifier Hearth under Thermal Loading using Finite Element Analysis

Umair Bin Asim, and Mubashir Ali Siddiqui

***Abstract*—**In this paper high stress regions in a small scale coal gasifier have been identified. Downdraft type gasifier is selected for this study due to its suitability for use in conjunction with reciprocating internal combustion engines. Major loading on the gasifier has been found to be due to thermal loads inside the reactor, which is in agreement with the temperature profiles developed by other researchers. Temperature in the oxidation region was maintained at 1200°C for tar breaking. The component most prone to failure, i.e. hearth is selected for the stress analysis as it experiences highest temperature due to direct contact with oxidation zone. Temperature distribution was applied as load in the analysis, resulting in deformation in hearth leading to stresses. Maximum von Mises' stress value was compared with yield strength of the material.

***Keywords*—**Coal Gasification, Hearth, Stress Analysis.

I. Introduction

GASIFICATION has been in used for a long time now. Solid fossil fuel has a drawback that it cannot be used in internal combustion engines and in various other applications. There have been times when shortage of conventional fuel pushed the nations to use gasification to power cars. Over one million vehicles in Europe ran with onboard gasifiers during WWII to make fuel from wood and charcoal, as gasoline and diesel were rationed or otherwise unavailable [1].

In addition to such scenarios gasification is being used as a favored option to generate electricity from coal. According to the Gasification Technologies Council, in 2007, around 144 gasification plants and 427 gasifiers were in operation worldwide, adding up to an equivalent thermal capacity of 56 GW_{th}, of which coal gasification accounted for approximately 31 GW_{th} [2]. Coal gasification has a large potential in future and thus generates a need to better understand the processes and technology involved. In addition to that, feasibility and optimization of the coal gasification systems need to be investigated as well.

Gasification is incomplete combustion. Instead of complete combustion of the fuel by oxidation, partially oxidized or reduced products are obtained. These products can then be oxidized in engines to produce useful shaft power. Gases produced by gasification goes by many names, Syngas, Town gas, wood gas, generator gas and producer gas etc., on the basis of their source, use and/or composition. Coal is carbonaceous fuel, containing carbon (C) as the main component. Coal has moisture content in varying quantities as well. Gasification converts coal into combustible carbon monoxide (CO) and Hydrogen (H_2) gases.

Gasification involves these distinct thermal processes; Drying, Pyrolysis, Combustion and Reduction [3]. These processes can occur in different sequences, depending upon the type of gasifier. Drying is the removal of moisture from solid fuel. Pyrolysis is the breakdown of coal into a combination of coke and tar at elevated temperatures. Combustion drives the gasification process by providing the heat required for reduction. CO_2 and H_2O are produced as a result of combustion, which will reduce under the action of heat and presence of coke. The process is termed as reduction that gives off a mixture of CO and H_2. A summary of these processes is given in Fig. 1.

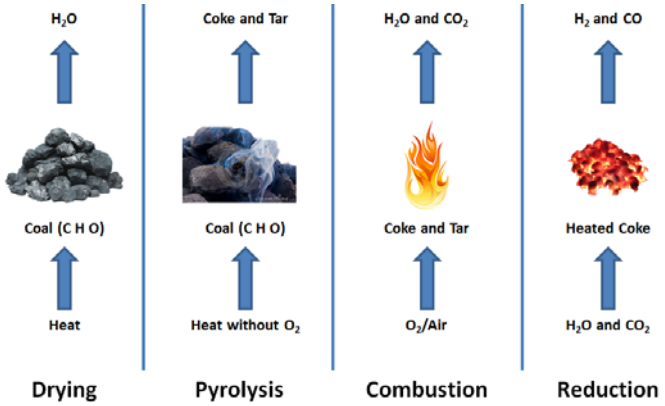

Fig. 1 Gasification Processes

Gasification is carried out in a chamber, called reactor, supplied with a limited supply of air, i.e. less than the amount required for complete oxidation. Heat required for reduction is generated by combustion of part of the fuel. Reduction gives out combustible gases. Gasifiers are made in fixed bed, fluidized bed or entrained flow types. In fixed bed type, solid fuel is added from the top of the gasifier and gases are either collected at the top (updraft type), bottom (downdraft type) or from sides (cross draft type). In fluidized bed, solid fuel is converted into granular form. Process occurs while the

Umair Bin Asim is with Mechanical Engineering Department of NED University of Engineering and Technology, Karachi, Pakistan. (Phone: 00923332458915; e-mail: umair.bin.asim@gmail.com).

Mubashir Ali Siddiqui is with Mechanical Engineering Department of NED University of Engineering and Technology, Karachi, Pakistan.

particles are suspended by the air blown upwards. Entrained flow gasifier uses pulverized coal and high temperatures that accelerate the carbon conversion rate [4].

A downdraft gasifier has been selected as it is the recommended type for small to medium scale energy generation applications. High char conversion, lower ash and tar carry over, quick response to load change and simple construction makes it suitable for the use with internal combustion engines [5].

Downdraft gasifier consists of a reactor, in which fuel is fed at the top. Process of drying starts at the top followed by the region where pyrolysis occurs just above the oxidation zone. Oxidation occurs at an area constriction, where air is injected into the reactor. The products of oxidation then pass over a hot bed of coal just below this constriction to reduce the oxidation products. The combustible gas achieved as a result of reduction is extracted from the bottom. A schematic of downdraft gasifier is shown in Fig 2.

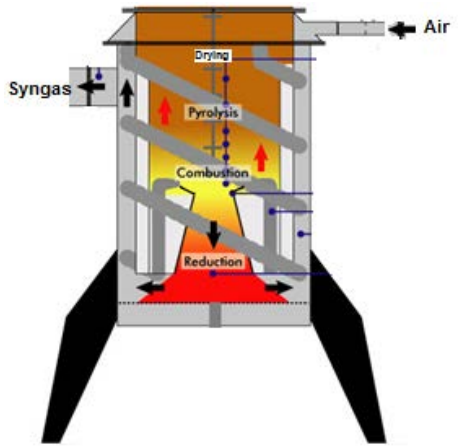

Fig. 2 Downdraft Gasifier

After careful consideration, it was observed that main source of loading in the gasifier is high temperature which reaches up to 1200˚C in the reactor. Maximum temperature in the reactor should be maintained at hearth for tar breaking. This high temperature induces thermal stresses in the hearth. These stresses can cause structural failure that can lead to inefficient operation, for which the hearth is selected for finite element analysis.

II. Governing Equations

Axial, radial and tangential stresses resulting from applied temperature loads can be found out using Equations (1), (2) and (3) [6].

$$\sigma_z = \frac{E.\alpha}{(1-\vartheta).r^2}.\left[\frac{2}{r_o^2-r_i^2}.\int_{r_i}^{r_0} T(r).r.dr - T(r)\right] \quad (1)$$

$$\sigma_r = \frac{E.\alpha}{(1-\vartheta).r^2}.\left[\frac{r^2-r_i^2 2}{r_o^2-r_i^2}.\int_{r_i}^{r_0} T(r).r.dr - \int_{r_i}^{r} T(r).r.dr\right] \quad (2)$$

$$\sigma_\theta = \frac{E.\alpha}{(1-\vartheta).r^2}.\left[\frac{r^2+r_i^2 2}{r_o^2-r_i^2}.\int_{r_i}^{r_0} T(r).r.dr + \int_{r_i}^{r} T(r).r.dr - T(r).r^2\right] \quad (3)$$

Where

- σ_r, σ_θ, σ_z are the radial, tangential and axial stress
- E is the modulus of elasticity
- α is the coefficient of thermal expansion
- ν is the Poisson's ratio
- T(r) is the radial temperature distribution
- r_o, r_i, and r are the outside radius, inside radius and the radius where stress is calculated

III. Methodology

Sequentially coupled thermal-structural analysis is a method by which thermal stress problems can be solved using finite element analysis. Wang et. al. [6] performed thermal stress analysis of eccentric cylinders. Temperature distribution attained through CFD analysis was applied at the nodes of the cylinders. Resulting stresses were computed through FEA.

A. Problem Specification

Sequentially coupled thermal-structural method was selected for analysis. As mentioned before hearth was selected for stress analysis, as it is in direct contact with the oxidation region where temperatures are around 1200°C.

1. Material Properties

Hearth is made of two 304 stainless steel plates of 3mm thickness. This steel grade is used for high temperature and corrosive environment applications. Also fabrication is relatively easier with this type of construction. Each of the plates is first rolled to make conical shape and then welded seam wise. These two plates are welded together to make hearth. The hearth is then welded to a flange of 5mm thick plate. Flange is then bolted to the reactor, due to which motion of flange is constrained. Grade 304 stainless steel properties are given in Table I.

TABLE I
PROPERTIES OF 304 STAINLESS STEEL [7]

Property	Value
Thermal Conductivity (W/m.K)	21.4
Coefficient of Thermal Expansion (10^{-6} m/m K)	18.7
Modulus of Elasticity (GPa)	193
Poisson's Ratio	0.3
0.2% Yield Strength (MPa)	290

2. Temperature Profile

Various tests were conducted on downdraft type gasifier to obtain the temperature profile for the efficient operation.

McKendry [8] discussed different fuel types and their effects in selecting suitable gasifier type. He also developed temperature distribution in a downdraft gasifier.

Olgun et. al. [9], discussed the importance of area constriction in downdraft gasifier to minimize tar quantity in produced gas. He also discussed temperature distribution in a small scale gasifier with different fuel types.

Zainal et. al. [10], discussed the effect of equivalency ratio on calorific value of gas and gas flow rate, along with the temperature distribution.

Dogru et. al. [11], recorded the temperature profile in the different zones of downdraft gasifier.

Temperature profile from [8], is given in Fig 3.

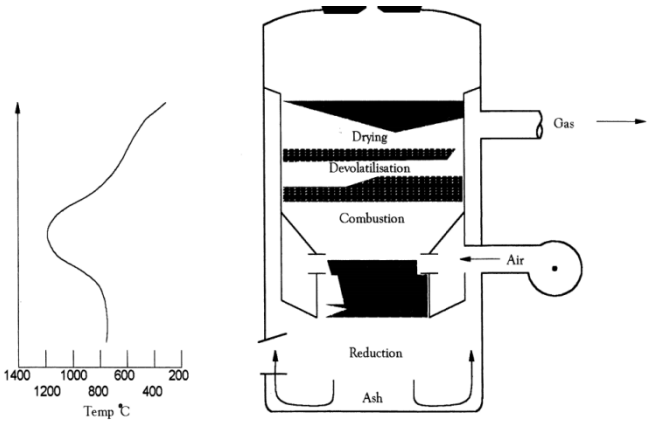

Fig. 3 Temperature Profile of Downdraft Gasifier [8]

The graph in Fig. 3 shows temperature distribution in a gasifier. Following data were extracted from the graph.

– Maximum temperature achieved at combustion region, i.e. at the top of the hearth at which maximum tar break up is possible, is 1200˚C.

– Maximum temperature at the throat of the hearth is 700˚C

– Maximum temperature at the base of the hearth is 800˚C

This temperature profile will be the input for the loads for this problem.

3. Assumptions

For the simplification of the problem, following assumptions have been made:

– Seamless, axisymmetric hearth

– Continuous welded joints

– Bolted joint between hearth's flange and the reactor bottom is assumed to be a displacement constraint at the bottom surface of flange

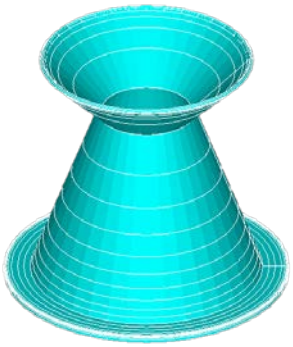

Fig. 4 CAD Model of Hearth

B. Modeling

A 3D CAD model, Fig. 4, was generated to get the coordinates required for hearth modelling. Obtained coordinates were modeled as keypoints which were joined together to form lines. The lines were then used to create area. As we are treating the problem as axisymmetric, there is no need to model the whole volume. But for better visualization this area can be rotated about its axis to form the complete 3D view of hearth.

C. Meshing

First thermal part of the problem was devised. As mentioned earlier, hearth is assumed to axisymmetric. So an axisymmetric ring element with a three-dimensional thermal conduction capability, i.e. Plane78 is selected for meshing the area. The element has one degree of freedom, temperature, at each node. The 8-node elements have compatible temperature shapes and are well suited to model curved boundaries.

Modeled area was meshed with Plane78 element, having thermal conductivity value as an input. Area was meshed with free, quadrilateral element. In start a coarse mesh was used, then refinement in high variation regions were done so as to achieve grid independence. Two iterations, after refining mesh each time, were done. Negligible variations were observed in the last iteration, after which mesh was finalized. Meshed geometry is saved as thermal environment, for further use in thermal analysis. Meshed area is illustrated in Fig. 5.

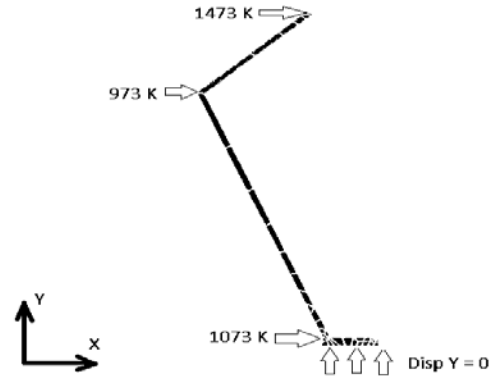

Fig. 5 Meshed Area with Temperature and Boundary Condition

Once the thermal environment is saved, element type is switched for structural analysis. Structure element type compatible with PLANE78 is PLANE83. PLANE83 is used for two-dimensional modeling of axisymmetric structures.

D. Solution

Thermal environment was called in the start. Temperature loads were applied according to the temperature profile given in Fig. 3.

Solution was performed for temperature distribution. Temperature distribution is shown in Fig. 6.

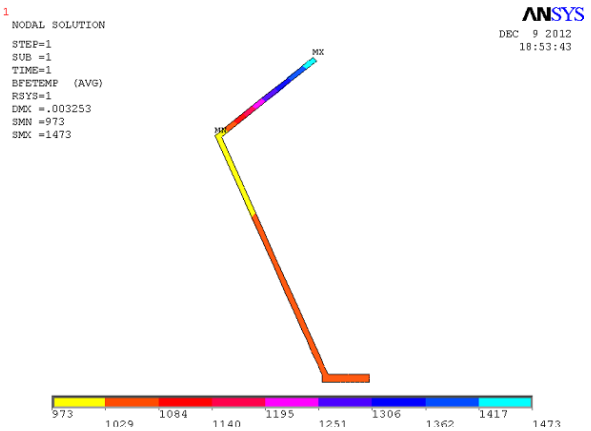

Fig. 6 Axisymmetric Temperature Distribution

Results from the thermal environment were then applied as temperature loads for the structural environment. In addition to that, displacement constraint was applied at the bottom of the hearth which is bolted to the bottom of the reactor.

Solution was carried out for the structural environment.

Solution was started with a coarse mesh. Results were recorded from the solution. In order to achieve mesh independence, mesh refinement was done. Some variations in the results were observed after solution was carried out with the first refinement cycle. Due to this variation, mesh was refined once again. Results showed negligible variation after this step, so the conclusion was drawn that the mesh independence has been achieved. In this way a total of three cycles were carried out, summary of which is given in Table II.

TABLE II
MESH REFINEMENT SUMMARY

Parameter	1st Run	2nd Run	3rd Run
Number of Elements	20	31	43
Solution time (s)	15	22	36
Max von Mises Stress (Pa)	156 x 10^6	195 x 10^6	197 x 10^6
Min von Mises Stress (Pa)	0.69 x 10^6	0.76 x 10^6	0.75 x 10^6

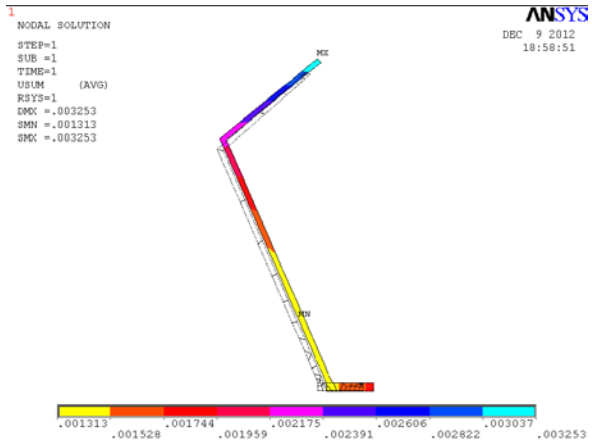

Fig. 7 Displacement vector sum with original geometry

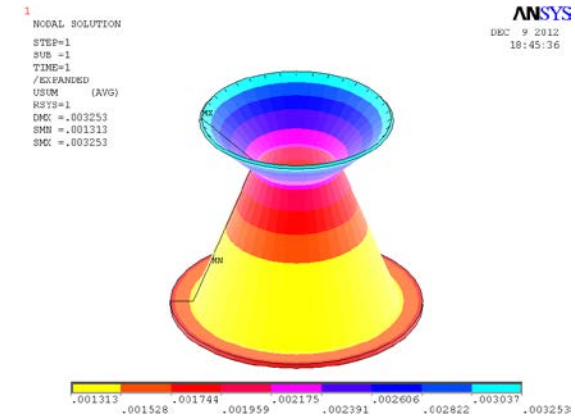

Fig. 8 Displacement vector sum of complete hearth

E. Post-processing

Results of the solution were plotted as contour plots.

1. Displacement

Displacements sum contours were plotted. As evident from Fig.7, maximum displacement is observed at the top of the hearth because this is the free end. Complete hearth is shown in the Fig. 8.

2. Stresses

Von Mises' stresses are plotted in form of contours. Von Mises' stress distribution for complete hearth is given in Fig. 9.

Maximum Von Mises' stress observed is 197 MPa at the throat region. In comparison with the yield strength of the material the factor of safety we are getting is 1.5.

IV. RESULTS AND DISCUSSION

A. Temperature Distribution

According to the applied temperature loads, maximum temperature i.e. 1473K is achieved at the inside wall, at the top of the hearth. Similarly minimum temperature is encountered at the inside wall, at the throat (Fig. 6). This distribution plot is shown in Fig. 10, where temperature is plotted on x-axis and axial location on y-axis for better visualization.

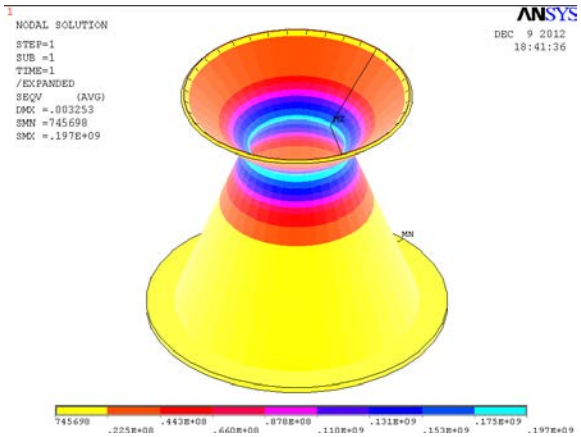

Fig. 9 Von Mises' Stress Distribution in Complete Hearth

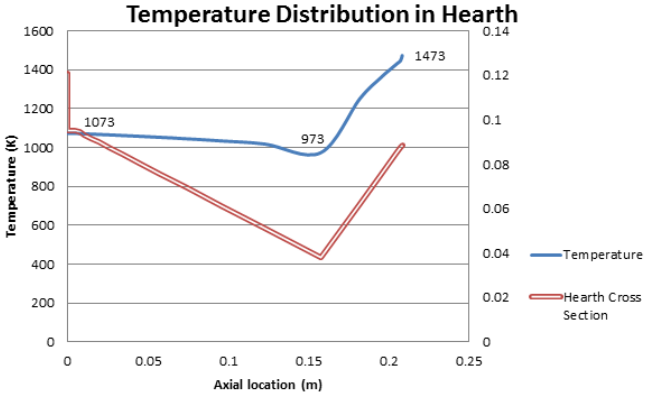

Fig. 10 Temperature distribution in Hearth

B. Displacements

1. Radial

Nodal displacements plot shows that the largest displacement in radial direction is at the inside wall of the throat. This is because material above and below the throat expands due to temperature which tries to squeeze the throat region inwards (shown as arrows on the Fig. 11). This result is also evident in Fig. 11. For this reason, the maximum displacement, mainly because of thermal expansion, was encountered there.

2. Axial

Maximum displacement in axial direction was achieved at the top of the hearth, i.e. around 3mm, because this is the free end of the hearth and can displace without any constraint.

3. Sum

Since the value of axial displacement at the top is well above the radial component at the bottom, displacement vector sum is maximum at the top of the hearth (Fig. 6).

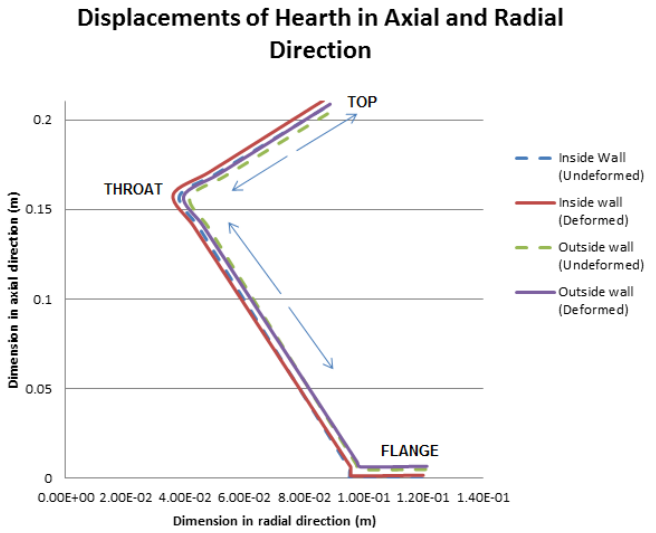

Fig. 11 Displacements of Hearth in Axial and Radial Direction

C. Stresses

1. Radial Stress

Stresses in radial directions have maximum value of 202 MPa in tension and 194 MPa in compression, both at the throat of the hearth. Throat inside wall is in tension, whereas outside wall is in compression. Rest of the hearth has stresses in the range of 18.3 MPa in compression to 25.7 MPa in tension. Minimum values are encountered in flange and at the top (free) end of the hearth. These observations are evident in Fig. 12. It is also observed that the values on inside and outside walls are opposite in direction at a given axial location.

2. Axial Stress

Stress distribution in axial direction showed that the maximum value in tension and compression are 48 MPa and 43 MPa, on inside and outside wall of throat region, respectively. Stresses ranging around 2 MPa in tension to around 8 MPa in compression are encountered in the rest of the hearth. Fig. 13 shows that maximum value of axial stress is less in comparison with radial and tangential components of stresses.

3. Tangential Stress

In tangential direction, maximum stresses observed in tension are well above than in compression. A value of 164 MPa was encountered in tension at the inside wall of the throat, Fig. 14. Tangential stresses in the rest of the hearth range from 12 MPa in tension to 13 MPa in compression.

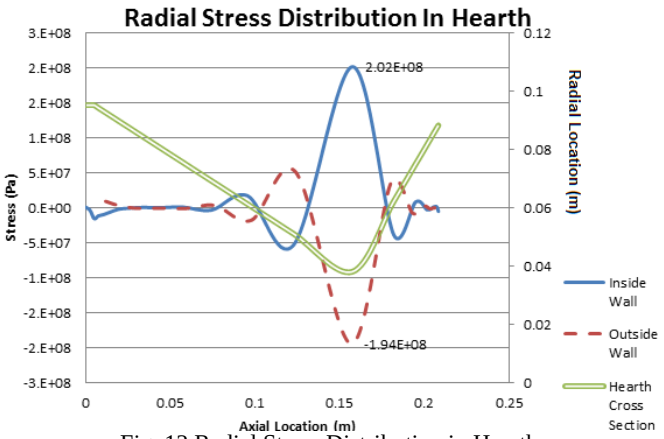

Fig. 12 Radial Stress Distribution in Hearth

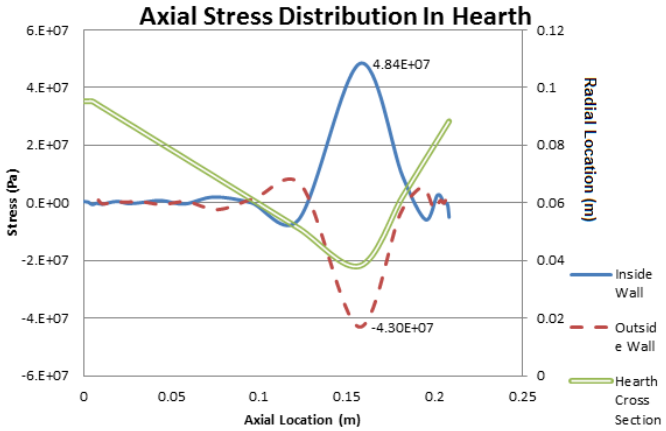

Fig. 13 Axial Stress Distribution

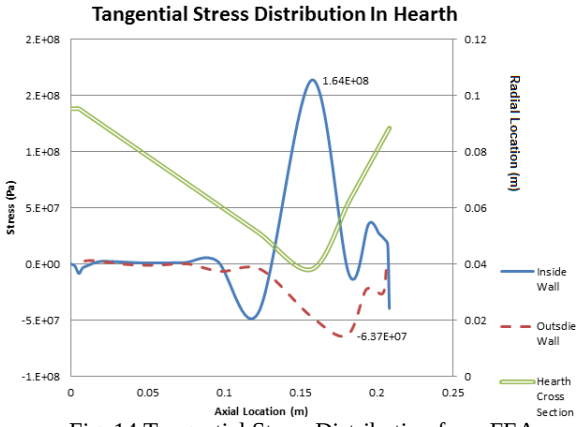

Fig. 14 Tangential Stress Distribution from FEA

4. Von Mises Stresses

Distribution of von Mises stresses (Fig. 9), on the basis of radial, axial and tangential stresses, shows that the maximum stresses are encountered at the throat region as expected on the basis of the results mentioned above. Maximum value of von Mises stress is 197 MPa, on the outer wall of the throat and 183 MPa on the outer wall. Besides these extremes, stress values in the range of 10 to 22 MPa were observed.

V. Conclusion

As observed from the results, it is concluded that the design is safe with a factor of safety of 1.5.

Maximum stress region is that of throat and hence extra caution must be taken to avoid any possible failure in this region.

These results are for the case when the top part of the hearth is free to displace. Thus special consideration must be taken to avoid any possible blockage in the free displacement. If such a situation arises, stresses will escalate which may lead to failure.

References

[1] H. LaFontaine, Zimmerman. "Construction of a simplified wood gas generator for fueling internal combustion engines in a petroleum emergency". *2nd Edition of BEF, Federal Emergency Management Agency*. March 1989.

[2] J. Childress, "Gasification Industry Overview: Addressing the Dash to Gas", *Gasification Technologies Council*. 2008.

[3] J. Koppejan and S. van Loo. "The Handbook of Biomass Combustion and Co-firing". *Earthscan* 2008.

[4] J. Philips, "Different Types of Gasifiers and Their Integration with Gas Turbines," *The Gas Turbine Handbook, NETL*. 2006.

[5] M. Dogru , C.R. Howarth, G. Akay, B. Keskinler, A.A. Malik, "Gasification of hazelnut shells in a downdraft gasifier" *Energy*, vol. 27, Issue 5, May 2002.

[6] F. Wang, Yong Shuai, Yuan Yuan, Guo Yang, Heping Tan. "Thermal stress analysis of eccentric tube receiver using concentrated solar radiation". *Solar Energy* 84 (2010) 1809–1815. http://dx.doi.org/10.1016/j.solener.2010.07.005

[7] Product data sheet, 304/304L Stainless Steel. AK Steel Corporation, Ohio.

[8] Peter McKendry. "Energy production from biomass (part 3): gasification technologies". *Bioresource Technology 83* (2002) 55–63 http://dx.doi.org/10.1016/S0960-8524(01)00120-1

[9] Hayati Olgun, Sibel Ozdogan, Guzide Yinesor. "Results with a bench scale downdraft biomass gasifier for agricultural and forestry residues". *Biomass and Bioenergy* 35 (2011) 572-580 http://dx.doi.org/10.1016/j.biombioe.2010.10.028

[10] Z.A. Zainal, Ali Rifau, G.A. Quadir, K.N. Seetharamu. "Experimental investigation of a downdraft biomass gasier". *Biomass and Bioenergy 23* (2002) 283 – 289 http://dx.doi.org/10.1016/S0961-9534(02)00059-4

[11] M. Dogru, C.R. Howarth, G. Akay, B. Keskinler, A.A. Malik. "Gasification of hazelnut shells in a downdraft gasifier". *Energy 27* (2002) 415–427 http://dx.doi.org/10.1016/S0360-5442(01)00094-9